Influence of Ammonium Phosphates on Gaseous Potassium Release and Ash-Forming Characteristics during Combustion of Biomass

ARTICLE *in* ENERGY & FUELS · APRIL 2015

Impact Factor: 2.79 · DOI: 10.1021/acs.energyfuels.5b00285

4 AUTHORS, INCLUDING:

Kuihua Han
Shandong University
45 PUBLICATIONS **263** CITATIONS
SEE PROFILE

Lu Chunmei
Shandong University
61 PUBLICATIONS **495** CITATIONS
SEE PROFILE

energy&fuels

Article

pubs.acs.org/EF

Influence of Ammonium Phosphates on Gaseous Potassium Release and Ash-Forming Characteristics during Combustion of Biomass

Hui Li,[†] Kuihua Han,*[,†,‡] Qian Wang,[†] and Chunmei Lu[†]

[†]School of Energy and Power Engineering, Shandong University, Jinan, Shandong 250061, People's Republic of China

[‡]Department of Mechanical Engineering, University College London, London WC1E 7JE, United Kingdom

ABSTRACT: The influence of ammonium phosphates, i.e., ammonium dihydrogen phosphate ($NH_4H_2PO_4$) and ammonium monohydric phosphate [$(NH_4)_2HPO_4$], on gaseous potassium (K) release was studied in a tube furnace during the combustion of maize straw (MS), cotton stalk (CS), and rice straw (RS). The gaseous potassium was absorbed by deionized water and measured by atomic absorption spectroscopy (AAS). The formed ashes were investigated using a combination of powder X-ray diffraction (XRD) and scanning electron microscopy combined with energy-dispersive X-ray spectroscopy (SEM−EDS) analyses after visual evaluation. The results show that the addition of $NH_4H_2PO_4$ and $(NH_4)_2HPO_4$ both decrease the potassium release ratio and show the same trends. $NH_4H_2PO_4$ and $(NH_4)_2HPO_4$ can be more effective with a higher initial potassium content. The release ratios of RS with $NH_4H_2PO_4$ and $(NH_4)_2HPO_4$ are 12.1 and 13.2% at 1000 °C, respectively, which both decrease most compared to the ratio of RS. The release ratio decreases as the PO_4^{3-}/K ratio increases from 0.5:1 to 4:1 at every temperature. The appropriate molar ratios of PO_4^{3-}/K are between 1:1 and 2:1. Surface melting and sintering are inhibited by the addition of $NH_4H_2PO_4$ and $(NH_4)_2HPO_4$. Ammonium phosphates can react with potassium to form potassium phosphates, and potassium calcium phosphates bound potassium in a K−Ca−P ternary system. A significant effect of $NH_4H_2PO_4$ on the microcosmic structure is noticed, and the ashes of the mixture show quite different morphologies because of the formation of phosphorus compounds. These phosphates, including $K_2CaP_2O_7$, K_3PO_4, and $KCaPO_4$, are high-melting-point compounds contributed to retaining potassium and preventing sintering of the formed ash.

1. INTRODUCTION

Biomass resources are now receiving more attention as a renewable and CO_2-neutral energy resource because of environmental considerations and the increasing demands of energy worldwide. Biomass resources, including wood and wood waste, agricultural crops and their waste byproducts, municipal solid waste, animal waste, waste from food processing, and aquatic plants and algae, can be converted to energy in various ways.[1−5] The increased use of biomass energy replacing conventional fossil fuels will contribute to mitigating the energy crisis and environmental pollution. As a large agricultural country, biomass energy has the potential to play a significant role in the future energy composition in China. From China's 12th Five-Year Plan for Biomass Energy Development, the ratio of biomass being used as energy is set to double the amount of biomass utilization from 5 to 10% until the end of 2015. The burning of biomass in air, i.e., combustion, is widely used to convert the chemical energy stored in biomass into heat, mechanical power, or electricity and also a relatively mature technology used in stoves, furnaces, boilers, steam turbines, etc.[6−8] However, biomass fuels rich in alkali metals used in biomass combustion systems have shown some negative influences on causing alkali-related operational problems, including fouling, sintering, bed agglomeration, and superheater corrosion.[9−11] Potassium (K) is the dominate type of alkali metal in the biomass because it is the essential element for the growth of plants. During combustion of biomass, potassium involved in complex transformation reactions with other ash-forming elements may form potassium salts, silicates, and phosphates retained in the ash and be released into the gas phase mainly through the sublimation of KCl.[12−16] Some of these potassium compounds or the eutectics with low melting points will melt and form viscous flow sintering and agglomeration on the surface of ash/char particles.[17−19] The volatilized potassium compounds in gaseous or aerosol phases can condense on heat-transferring surfaces and deposit as particles. Because potassium release is often accompanied by chlorine, high levels of KCl in deposits will accelerate the corrosion.[20−22]

There are various approaches to reduce these potassium-related operational problems during combustion of biomass. Co-combustion with other types of fuels and mixing with additives have been proven promising and efficient methods to change the fuel composition concerning to its inorganic content. These fuels and additives rich in sulfur and other mineral metals, such as calcium, aluminum, and magnesium, can capture released potassium and improve the sintering characteristics of biomass by forming species with high melting points.[23−32] Previous studies mainly focus on biomass with a low phosphorus content, and the effect of additives based on phosphorus has not been well investigated. Relatively few studies focusing the influence of phosphorus on potassium behavior during combustion of biomass have been proposed. Rapeseed meal (RM) rich in phosphorus mixed with bark was employed by Boström et al.[33] in a bubbling fluidized bed. A significant difference in the mechanisms of bed agglomeration

Received: February 5, 2015
Revised: March 20, 2015
Published: March 20, 2015

DOI: 10.1021/acs.energyfuels.5b00285
Energy Fuels 2015, 29, 2555−2563

Table 1. Ultimate, Proximate, and Potassium Analyses of the Samples (wt %, on an Air-Dried Basis)

	proximate analysis				ultimate analysis					alkali metal
sample	M^a	A^b	FC^c	V^d	C	H	O	N	S	K
MS	7.84	8.63	14.37	69.16	43.31	5.78	33.07	1.06	0.31	1.80
CS	8.22	14.74	15.16	61.88	41.84	5.41	28.22	1.30	0.27	1.42
RS	4.34	15.19	14.71	65.76	39.87	5.46	33.60	1.25	0.29	2.09

$^a M$ = moisture. $^b A$ = ash. $^c FC$ = fixed carbon. $^d V$ = volatile.

Table 2. Content of Ash of Biomass (wt %)

sample	Na_2O	MgO	Al_2O_3	SiO_2	P_2O_5	SO_3	Cl	K_2O	CaO	Fe_2O_3	others	total
MS	0.31	6.85	2.10	36.62	3.59	4.74	5.71	28.36	9.11	2.06	0.55	100
CS	3.74	7.13	8.94	30.80	4.14	4.79	2.90	17.50	15.23	3.94	0.89	100
RS	0.74	2.74	0.34	58.81	2.08	3.09	5.63	20.45	3.89	0.52	1.72	100

for RM was observed that very thin and discontinuous layers were together with isolated partly melted bed ash particles instead of the ubiquitous continuous layers on the bed grains found during combustion of woody biomass. It could be explained that the considerable higher affinity for base cations of phosphorus than silicon would prevent the present basic oxides from attacking the quartz bed grains and forming agglomeration at low temperatures. Grimm et al.[34,35] confirmed that the addition of phosphorus-rich fuels and phosphoric acid could convert the available fuel ash basic oxides into phosphates and change the alkali distribution from being dominated by amorphous K silicate coarse ash fractions and fine particulate KCl to a system dominated by crystalline coarse ash of K−Ca/Mg phosphates and fine particulate K_2SO_4. Li et al.[36] selected calcium phosphate [$Ca_3(PO_4)_2$] as a model phosphorus compound in municipal sewage sludge ash to study the influence of phosphorus on potassium behavior. Results showed that $Ca_3(PO_4)_2$ could absorb and react with potassium compounds to form $Ca_{10}K(PO_4)_7$ with a high melting point. Skoglund et al.[37] found that the addition of K_2CO_3 and $CaCO_3$ would affect the speciation of phosphorus, and phosphorus was identified as whitlockite [$Ca_9(K, Mg, Fe)(PO_4)_7$] enriched in the bed ash. However, the formation of low-melting-point potassium phosphate, i.e., KPO_3, was also indicated to play an important role in accelerating bed agglomeration during combustion of biomass with a high phosphorus content.[38,39] Considering the discrepancies, it is important to gain a more precise and thorough understanding on the influence of phosphorus on potassium behavior during combustion of biomass.

Ammonium phosphates were employed as phosphorus additives in this study. In comparison to the phosphorus acid with high acidity and calcium phosphates chosen in previous studies, ammonium phosphates introduce no other metal cations and have no direct influence on the raw materials during the mixing process. Using ammonium phosphates as additives during biomass combustion is a good way to learn more about phosphate chemistry. The performance of ammonium phosphates will propose meaningful suggestions and then be used in more real situations, where co-firing of fuels with low- and high-P contents is usually applied. Furthermore, ammonium phosphates are usually used as fertilizers. Reuse of ashes containing phosphates will decrease the dependency of mineral-bound nutrient sources, which will benefit long-term sustainability. The main object was therefore to determine the influence of ammonium phosphates on gaseous potassium release and ash-forming characteristics of biomass fuels.

2. MATERIALS AND METHODS

2.1. Samples. Three kinds of typical biomass, maize straw (MS), cotton stalk (CS), and rice straw (RS), were used in this study. These biomass resources with a high potassium content are widely used for biomass molding fuel, heat, and power generation and heating and cooking in north China, which were grown in rural areas in Dezhou, Shandong, China. All of the received biomass were pulverized and sieved with a sieve of 80 mesh (i.e., 180 μm). Table 1 shows the results of the proximate and ultimate analyses. The potassium content in the raw materials measured by inductively coupled plasma−atomic emission spectrometry (ICP−AES, Thermo Fisher Scientific, IRIS Advantage) is also listed in Table 1. Ammonium dihydrogen phosphate ($NH_4H_2PO_4$) and ammonium monohydric phosphate [$(NH_4)_2HPO_4$] (Kemiou Chemical Reagent Co.), which were analytically pure were mechanically blended with the raw materials with a fixed molar ratio and stirred for 1 h, respectively. The ash content of three raw materials analyzed with an X-ray fluorescence spectrometer (XRF, Rigaku Co., ZSX Primus II) is listed in Table 2.

2.2. Experimental Methods. The gaseous potassium release experiments were conducted in a tube furnace shown in Figure 1. The experimental setup was made up of a gas-feeding system, a reaction system, and a gas-absorbing system. The steel cylinder was used to supply air for combustion, which was filled by an air compressor through an air filter relief-pressure valve. The volumetric flow rate of air was controlled by the rotameter. The reaction system included a corundum tube connected with silicon tubes and an electrical furnace.

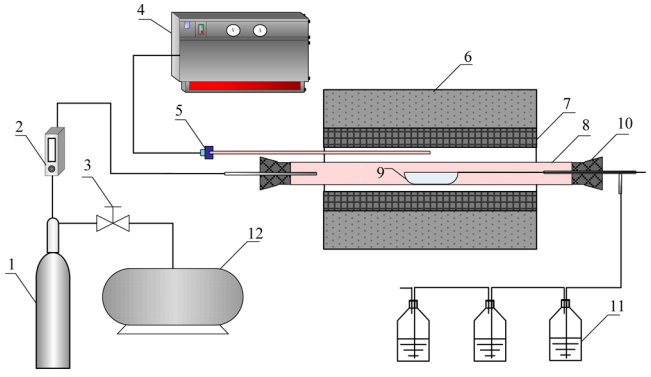

Figure 1. Schematic diagram of the gaseous potassium release experiment system: (1) air steel cylinder, (2) rotameter, (3) air filter relief-pressure valve, (4) temperature controller, (5) thermocouple, (6) insulating layer, (7) electric heating element, (8) corundum tube, (9) alumina boat, (10) rubber plug, (11) gas-washing bottle, and (12) air compressor.

DOI: 10.1021/acs.energyfuels.5b00285
Energy Fuels 2015, 29, 2555−2563

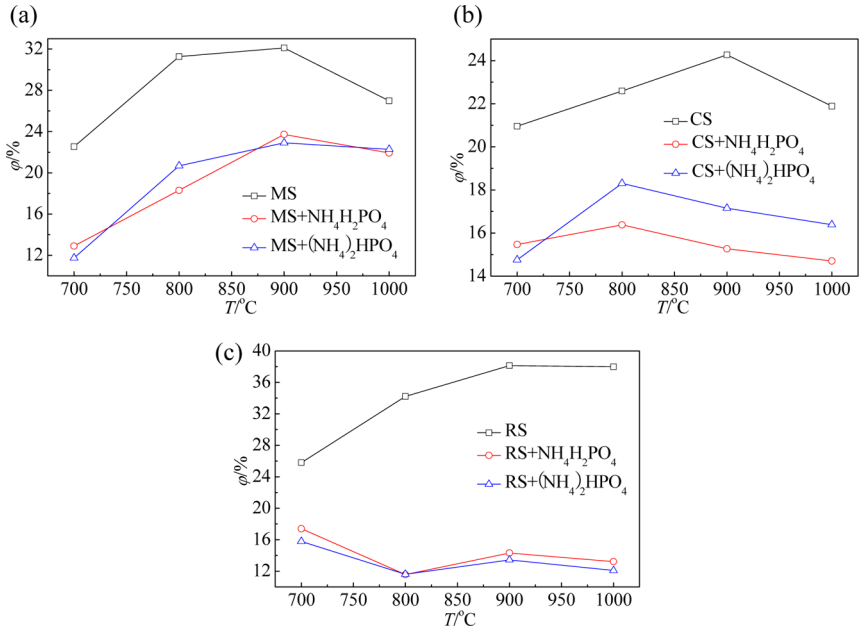

Figure 2. Ammonium phosphates on gaseous potassium release.

The inner diameter and length of the tube were 17 and 550 mm, respectively. The rubber plugs of both ends were traversed by quartz tubes to transport the air and flue gas, the inner diameter of which was 6 mm. The electrical element of the furnace was composed of silicon carbide rods with a rated power of 3 kW. The reaction temperature, from 700 to 1000 °C, was controlled by a proportional integral derivative (PID) temperature controller, whereas the power of the heater was controlled by a solid-state relay (SSR) power controller. The length of the constant temperature zone of the furnace was about 150 mm. The size of the alumina boat was 80 × 12 × 9 mm. The gas-absorbing system was made of three gas-washing bottles. Each bottle was injected with ~150 mL of deionized water to absorb the gaseous potassium before the experiment.

In each batch, the alumina boat containing 250 ± 0.5 mg of sample was quickly pushed into the constant temperature zone of the reactor at each reaction temperature and then the plug was tightened; meanwhile, air supplied by the cylinder was introduced into the tube at a continuous flow of 400 mL/min. The combustion time was set for 1 h, which was enough for the samples to burn out. After the experiment, the tube was taken out and cooled to room temperature under ambient conditions. The corundum tube and connecting silicon tubes were rinsed with the deionized water. The absorbing solution and washing water were transferred into a 1000 mL volumetric flask and then diluted with deionized water to volume. The concentration of potassium in the solution was measured by atomic absorption spectroscopy (AAS, Beijing Purkinje General Instrument Co., Ltd., TAS-990). The experiment under any given condition was usually carried out more than twice. The results were fairly uniform between each patch, and the relative error was less than 5%. The potassium release ratio was calculated by

$$\varphi = \frac{\omega V}{mM} \times 100\% \quad (1)$$

where φ was the potassium release ratio (%), ω was the potassium concentration in the diluted absorbing solution (mg/mL), V was the volume of the diluted absorbing solution (1000 mL in each batch), m was the weight of biomass in the sample (mg), and M was the content of potassium element in biomass (%).

The formed ash samples in the alumina boat after each batch were first visually evaluated, then ground, homogenized, and collected for further analyses. The chemical compositions were qualitatively analyzed by powder X-ray diffraction (XRD, Bruker Instrument Co., Ltd., Advanced D8) for identification of main crystalline phases. The XRD data collections were performed in θ–θ mode, which used a Cu radiation source with electricity at 100 mA and voltage at 40 kV. The 2θ range was from 10° to 90° with a step size of 0.1° and scanning speed of 4° min^{-1}. Then, the data were further analyzed by MDI Jade 5.0 to obtain the information on the crystalline phases. The samples were also mounted on carbon tapes and analyzed by scanning electron microscopy (SEM, Carl Zeiss AG., Supra 55) to observe the morphology of the samples. Semi-quantitative area analyses by energy-dispersive X-ray spectroscopy (EDS) combined with SEM were carried out for representative areas to obtain more detailed microchemistry information.

3. RESULTS AND DISCUSSION

3.1. Ammonium Phosphate on Gaseous Potassium Release. Figure 2 shows the experimental results of $NH_4H_2PO_4$ and $(NH_4)_2HPO_4$ on gaseous potassium release with the molar ratio of 1:1 PO_4^{3-}/K at 700–1000 °C. It is seen that the gaseous potassium release ratio of the raw materials increases to a maximum as the reactor temperature increases to 900 °C. The release ratios of MS, CS, and RS are 32.1, 24.3, and 38.1% at 900 °C, respectively. Above 900 °C, the release ratios of MS and CS decrease obviously, while the ratios of RS change little. It has been reported that potassium is closely correlated with chlorine through sublimation of KCl before the complete dechlorination at ~800 °C. Then, the high-temperature potassium release is thought to be governed by the thermal decomposition of K_2CO_3, leading to the increased release of K or KOH to the gas phase. However, the dissociation of K_2CO_3 has to compete with the incorporation of K to a ceramic phase. Some chemical compositions, such as Si and Al, may play a role in the retention mechanism of K, leading to the decrease of the potassium release ratio above 900 °C.[20,40] This will be verified by composition analysis afterward. The addition of $NH_4H_2PO_4$ and $(NH_4)_2HPO_4$ both decrease the ratio, confirming the potassium capture ability of ammonium phosphate, and show the same trends, presenting little difference on the gaseous potassium release. Although $NH_4H_2PO_4$ is more effective in potassium capture with a lower release ratio for CS and $(NH_4)_2HPO_4$ is more effective for RS, the differences of the release ratios are all less than 2% and can

DOI: 10.1021/acs.energyfuels.5b00285
Energy Fuels 2015, 29, 2555–2563

be ignored. The trends of potassium release ratios of MS and CS with $NH_4H_2PO_4$ and $(NH_4)_2HPO_4$ are similar to those of raw materials. RS with $NH_4H_2PO_4$ and $(NH_4)_2HPO_4$ show different trends with the ratio decreasing as the reactor temperature increases to 800 °C. $NH_4H_2PO_4$ and $(NH_4)_2HPO_4$ are more effective to RS for the decrease of the release ratios at every temperature of 8.4−25.9%, which is much higher than MS (4.7−13.0%) and CS (4.3−9.0%). It is consistent with the order of the potassium content in the raw materials, indicating that $NH_4H_2PO_4$ and $(NH_4)_2HPO_4$ can be more effective with a higher initial potassium content. The release ratios of RS with $NH_4H_2PO_4$ and $(NH_4)_2HPO_4$ are 12.1 and 13.2% at 1000 °C, respectively, which both decrease most compared to the ratio of RS.

The samples chosen for the experiments of the PO_4^{3-}/K ratio on gaseous potassium release were RS with $NH_4H_2PO_4$, and the molar ratios of PO_4^{3-}/K were 0.5:1, 1:1, 2:1, and 4:1, respectively. Figure 3 illustrates the results of the release ratios

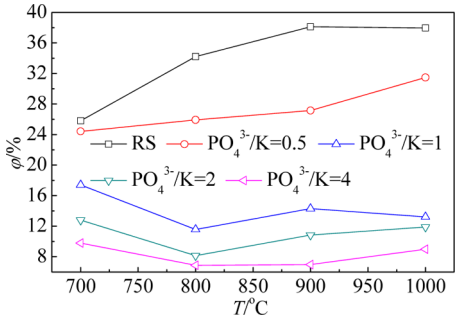

Figure 3. PO_4^{3-}/K ratios on gaseous potassium release.

with different PO_4^{3-}/K ratios at 700−1000 °C. The release ratio decreases as the PO_4^{3-}/K ratio increases from 0.5:1 to 4:1 at every temperature. As the molar ratio increases from 0.5:1 to 1:1, the release ratio decreases dramatically, while it decreases a little as the PO_4^{3-}/K ratio increases from 1:1 to 4:1. It reveals that ammonium phosphates need to be excessive to capture potassium in the ash significantly. The lowest release ratios of the samples with molar ratios of 1:1, 2:1, and 4:1 all appear at 800 °C, and they are 11.6, 7.1, and 6.9%, respectively. Nevertheless, the formed ash samples with the molar ratio of 4:1 PO_4^{3-}/K are observed to be melted and sintered when the temperature is above 900 °C. Too much excessive $NH_4H_2PO_4$ may also have some negative influences on the combustion characteristics of biomass, which will increase the cost of operation. Above all, the molar ratios of PO_4^{3-}/K between 1:1 and 2:1 can be adopted to obtain a satisfying potassium release ratio. The mechanisms of the inhibition effect of ammonium phosphates on gaseous potassium release may be related to the interaction between ammonium phosphates and the chemical compositions in the raw materials, which will be discussed in section 3.2.

3.2. Ammonium Phosphate on Ash-Forming Characteristics. Figure 4 shows the images of formed ash samples of RS and RS with $NH_4H_2PO_4$ and $(NH_4)_2HPO_4$ with the molar ratio of 1:1 PO_4^{3-}/K at 700−1000 °C. It can be seen that the ashes of RS with $NH_4H_2PO_4$ and $(NH_4)_2HPO_4$ are alike but very different from that of the raw materials at every temperature. The RS ash shrinks as the temperature increases, and the appearance is dark gray and loose, resembling the original appearance, at 700 °C, black at 800 and 900 °C but

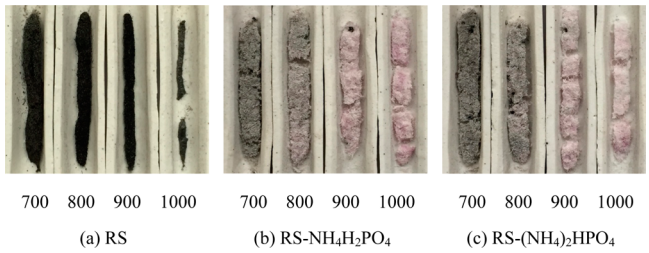

Figure 4. Images of formed ash samples at different temperatures (°C).

from partial sintering with fragile structures to hard sintering with partial melting, and metallic gray for when it is completely melted at 1000 °C. It is known that, during the process of biomass combustion, the organic matter, such as cellulose and lignin, decomposes into carbon. In each batch, the sample was suddenly introduced into the tube maintained at a high temperature. This caused simultaneous oxidation of carbon and formation of low-melting-point potassium salts, followed by surface melting. Once carbon is entrapped in the potassium-rich melt, it cannot be oxidized because it is not in direct contact with air. Therefore, the ashes of RS are observed to be black.[41] The shapes of the ashes of RS with $NH_4H_2PO_4$ and $(NH_4)_2HPO_4$ change little, and all resemble the original appearance from 700 to 1000 °C. The ashes stay loose until they are partly sintered at 1000 °C. However, the color of the formed ash samples changes gradually from gray to white gray mixed with light purple, confirming the existence of phosphates. According to the appearance, surface melting and sintering are inhibited by the addition of $NH_4H_2PO_4$ and $(NH_4)_2HPO_4$, indicating some high-melting-point potassium salt formation during the combustion process. Some black particles observed in the ashes below 900 °C may be due to an uneven distribution of ammonium phosphates caused by mechanical blending.

Figure 5 shows XRD patterns of the formed ashes of RS and RS with $NH_4H_2PO_4$ and $(NH_4)_2HPO_4$ at different temperatures after visual evaluation. SiO_2 is the main phase identified in all of the ash samples because it is the main composition in the raw materials according to the XRF results. Three kinds of SiO_2, i.e., quartz, tridymite, and cristobalite, are identified in the ashes of the samples. However, quartz is only detected in all of the three formed ashes at 700 °C, and cristobalite is only detected above 900 °C in the ashes of RS with $NH_4H_2PO_4$ and $(NH_4)_2HPO_4$. It can be seen from Figure 5a that evident peaks for KCl are observed in the RS ash, and it is the only crystalline phase detected with strong intensity at 700 °C. The peak number and intensity for KCl decrease dramatically at elevated temperatures, and no KCl is identified above 900 °C for the formation and sublimation of KCl terminated after complete dechlorination at ~800 °C. Some potassium sulfates, i.e., K_2SO_4 and $K_2S_2O_7$, are also found with a few weak peaks below 1000 °C, and the only crystalline phases identified are SiO_2 and $CaSO_4$ at 1000 °C. However, the potassium release ratio of the RS changes little from 900 to 1000 °C. It suggests the formation of some amorphous potassium compounds that cannot be identified by XRD at 1000 °C. The formed ashes of RS with $NH_4H_2PO_4$ and $(NH_4)_2HPO_4$ illustrated in panels b and c of Figure 5 show quite different XRD patterns from that of RS because of the complicated interactions among the major ash-forming elements from RS and the added ammonium phosphates. Similar crystalline compositions are identified in

DOI: 10.1021/acs.energyfuels.5b00285
Energy Fuels 2015, 29, 2555−2563

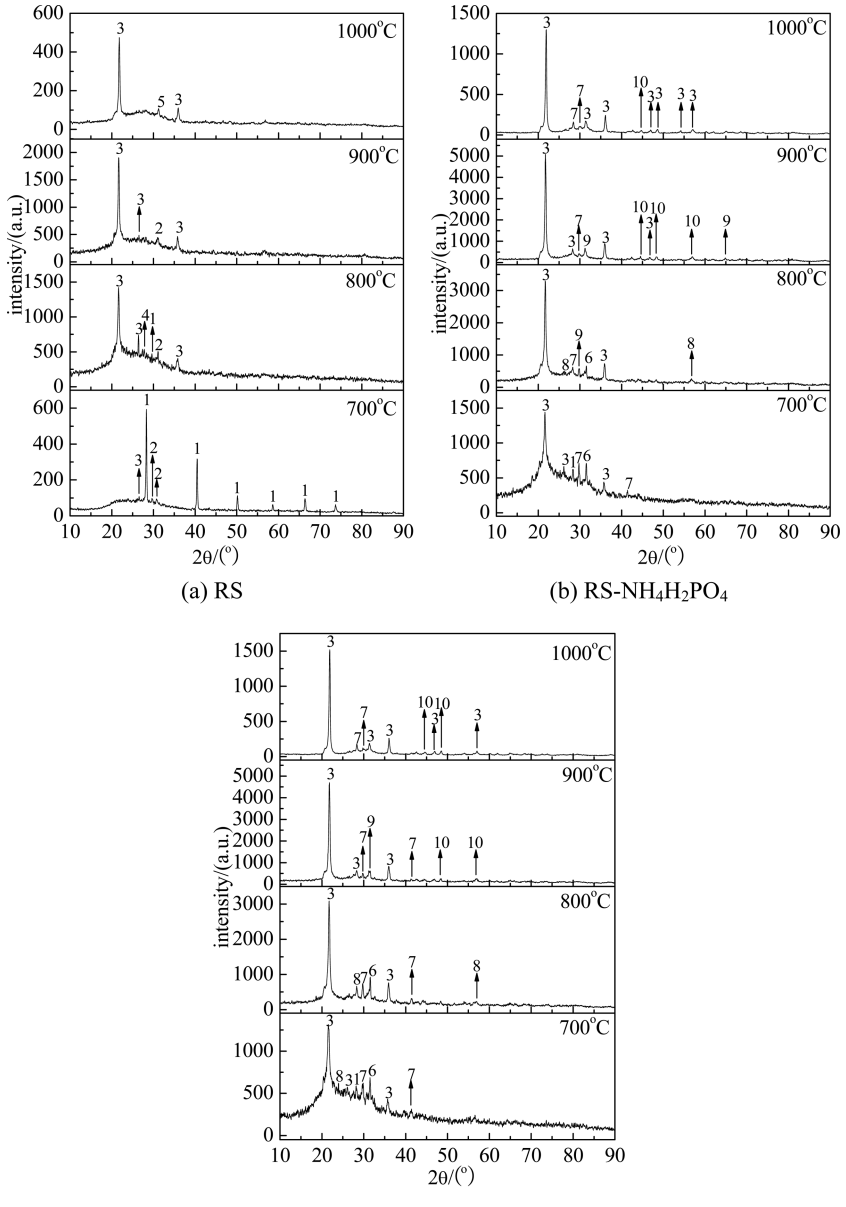

Figure 5. XRD patterns of the formed ash samples: (1) KCl, (2) K_2SO_4, (3) SiO_2, (4) $K_2S_2O_7$, (5) $CaSO_4$, (6) $CaCl_2$, (7) $K_2CaP_2O_7$, (8) $(KPO_3)_n$, (9) K_3PO_4, and (10) $KCaPO_4$.

the ashes of RS with $NH_4H_2PO_4$ and $(NH_4)_2HPO_4$ at every temperature, which is consistent with the results of the gaseous potassium release in section 3.1. Incomplete crystallization is shown at 700 °C with the addition of ammonium phosphates because there are broad humps and indented peaks in the baseline. The peaks for potassium sulfates cannot be distinguished, and only one peak for KCl is identified at 700 °C. The major minerals formed are $CaCl_2$, $K_2CaP_2O_7$, $(KPO_3)_n$, K_3PO_4, and $KCaPO_4$. It is consistent with that if there is a competition for potassium among the acidic oxide components, such as P_2O_5, SO_2/SO_3, and SiO_2; potassium phosphates are first formed.[34] The formation of these potassium phosphates and potassium calcium phosphates also indicates that ammonium phosphates are active to react with potassium via different reaction paths. These phosphates, except $(KPO_3)_n$, are high melting point compounds ($K_2CaP_2O_7$ at 1143 °C, K_3PO_4 at 1620 °C, and $KCaPO_4$ at 1560 °C)[42] and non-volatile. Potassium bound as phosphates, which mainly exists in the K−Ca−P ternary system, will contribute to the decrease of the potassium release ratio. $(KPO_3)_n$ is of little help with potassium capture because $(KPO_3)_n$ melts at 810 °C and will release potassium as well at elevated temperatures. According to the temperatures of these products identified, i.e., $K_2CaP_2O_7$ at 700−1000 °C, $(KPO_3)_n$ below 800 °C, K_3PO_4 at 800 and 900 °C, and $KCaPO_4$ above 900 °C, the reactions between the potassium compounds and $NH_4H_2PO_4$ can be inferred by the following. Some simplification is assumed that the main potassium compound involved in the reaction differs with temperatures based on the previous studies (KCl below 800 °C and K_2O and KOH above 800 °C),[20] regardless of the reactions among the formed potassium phosphates and potassium calcium phosphates.

DOI: 10.1021/acs.energyfuels.5b00285
Energy Fuels 2015, 29, 2555−2563

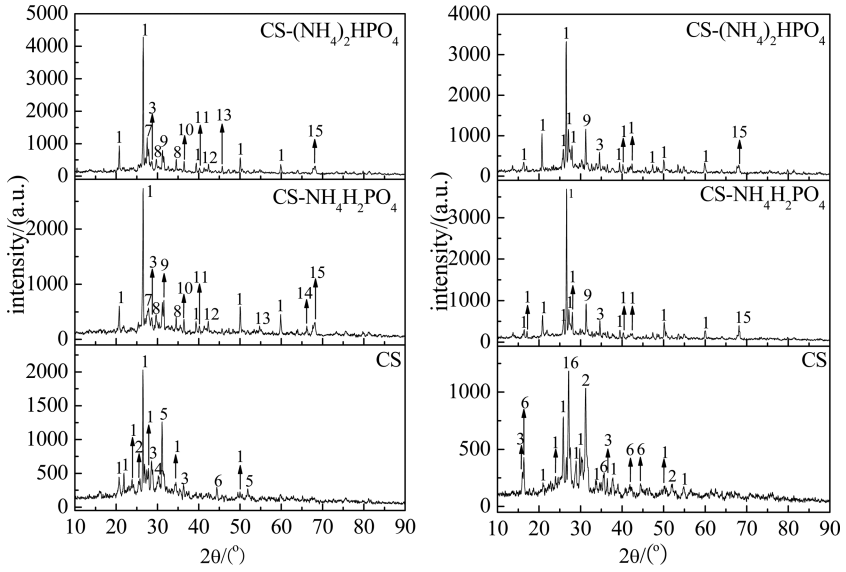

(a) 800 °C (b) 1000 °C

Figure 6. XRD patterns of the formed ash samples: (1) SiO_2, (2) $CaSO_4$, (3) $KAlSiO_4$, (4) K_2SO_4, (5) $Ca_2MgSi_2O_7$, (6) $KFeSi_2O_6$, (7) $(KPO_3)_n$, (8) $KCa(PO_3)_3$, (9) K_3PO_4, (10) $KMg(PO_3)_3$, (11) $Ca_2P_2O_7$, (12) $Fe(PO_3)_2$, (13) $Fe(PO_3)_3$, (14) $CaMg(SiO_3)_2$, (15) $KCaPO_4$, and (16) $KFeSi_3O_8$.

$$2NH_4H_2PO_4 + 2KCl + CaO \rightarrow K_2CaP_2O_7 + 2NH_4Cl + 2H_2O \quad (R1)$$

$$nNH_4H_2PO_4 + nKCl \rightarrow (KPO_3)_n + nNH_4Cl + nH_2O \quad (R2)$$

$$2NH_4H_2PO_4 + K_2O + CaO \rightarrow K_2CaP_2O_7 + 2NH_3 + 3H_2O \quad (R3)$$

$$2NH_4H_2PO_4 + 3K_2O \rightarrow 2K_3PO_4 + 2NH_3 + 3H_2O \quad (R4)$$

$$2NH_4H_2PO_4 + K_2O + CaO \rightarrow 2KCaPO_4 + 2NH_3 + 3H_2O \quad (R5)$$

$$2NH_4H_2PO_4 + 2KOH + CaO \rightarrow 2K_2CaP_2O_7 + 2NH_3 + 4H_2O \quad (R6)$$

$$NH_4H_2PO_4 + 3KOH \rightarrow K_3PO_4 + NH_3 + 3H_2O \quad (R7)$$

$$NH_4H_2PO_4 + KOH + CaO \rightarrow KCaPO_4 + NH_3 + 2H_2O \quad (R8)$$

The exact mechanisms need to be further clarified, and these reactions above can only be seen as overall reactions. As revealed by the reactions, unwanted NH_3 is produced as a byproduct. NH_3 is toxic and corrosive and can be oxidized into NO at elevated temperatures.[43] Further studies need to be performed to eliminate the polluted byproduct.

It can be seen from Table 2 that the contents of the ash-forming elements of Mg, Al, and Fe in the ashes of MS and CS are much higher than those in RS. These elements may compete with potassium to react with PO_4^{3-} and have some influence on gaseous potassium release. Figure 6 shows XRD patterns of the formed ashes of CS and CS with $NH_4H_2PO_4$ and $(NH_4)_2HPO_4$ with the molar ratio of 1:1 PO_4^{3-}/K at 800 and 1000 °C. Many complex compounds are identified in the individual and mixed ash samples. Quartz, tridymite, stishovite, and coesite are four kinds of SiO_2 identified, and no peaks for cristobalite are detected, which is different from the ashes of RS with $NH_4H_2PO_4$ and $(NH_4)_2HPO_4$. Only quartz and tridymite are detected in the ashes of the samples at 800 °C, and stishovite is only detected in the ash of CS at 1000 °C. For the CS ash, $KAlSiO_4$, $KFeSi_2O_6$, and $KFeSi_3O_8$ are the main potassium compounds identified. $KAlSiO_4$, which has a high melting point of 1600 °C, is an expected component formed when using kaolin as additives to retain potassium.[27,28] $KAlSiO_4$, $KFeSi_2O_6$, and $KFeSi_3O_8$ are all hard to volatilize and make the potassium release ratio of CS lower than RS. Mg and Ca have little effect on potassium capture without PO_4^{3-} from $NH_4H_2PO_4$ and $(NH_4)_2HPO_4$ because only $CaSO_4$ and $Ca_2MgSi_2O_7$ are identified in the CS ash not bound with potassium. When mixed with $NH_4H_2PO_4$ and $(NH_4)_2HPO_4$, phosphorus exists as phosphorus compounds in the form of $(KPO_3)_n$, $KCa(PO_3)_3$, K_3PO_4, $KMg(PO_3)_3$, $Ca_2P_2O_7$, $Fe(PO_3)_2$, $Fe(PO_3)_3$, and $KCaPO_4$ at 800 °C, but the peaks for $KFeSi_2O_6$ and $KFeSi_3O_8$ are not found. The formation of $Ca_2P_2O_7$, $Fe(PO_3)_2$, and $Fe(PO_3)_3$ means depletion of PO_4^{3-}, which is negative for potassium capture. As demonstrated in Figure 6b, in comparison to crystalline phases observed at 800 °C, K_3PO_4 and $KCaPO_4$ are the only phosphorus compounds identified at 1000 °C. It is consistent with the results obtained in the ashes of RS with $NH_4H_2PO_4$ and $(NH_4)_2HPO_4$. It indicates that potassium bound as phosphates in the K−Ca−P ternary system will not be influenced by the other ash-forming elements, i.e., Mg and Fe, at elevated temperatures.

The ashes of RS and CS are observed melted and sintered at 1000 °C, and some amorphous materials are often related to the melted fractions that cannot be directly identified by XRD. It is necessary to obtain more information about these amorphous phases to clarify the underlying ash formation mechanisms. Indirect evidence of their existence is obtained by comparing results from SEM−EDS and XRD analyses to provide supplementary microchemistry information. Panels a−d of Figure 7 show representative SEM micrographs of the

DOI: 10.1021/acs.energyfuels.5b00285
Energy Fuels 2015, 29, 2555−2563

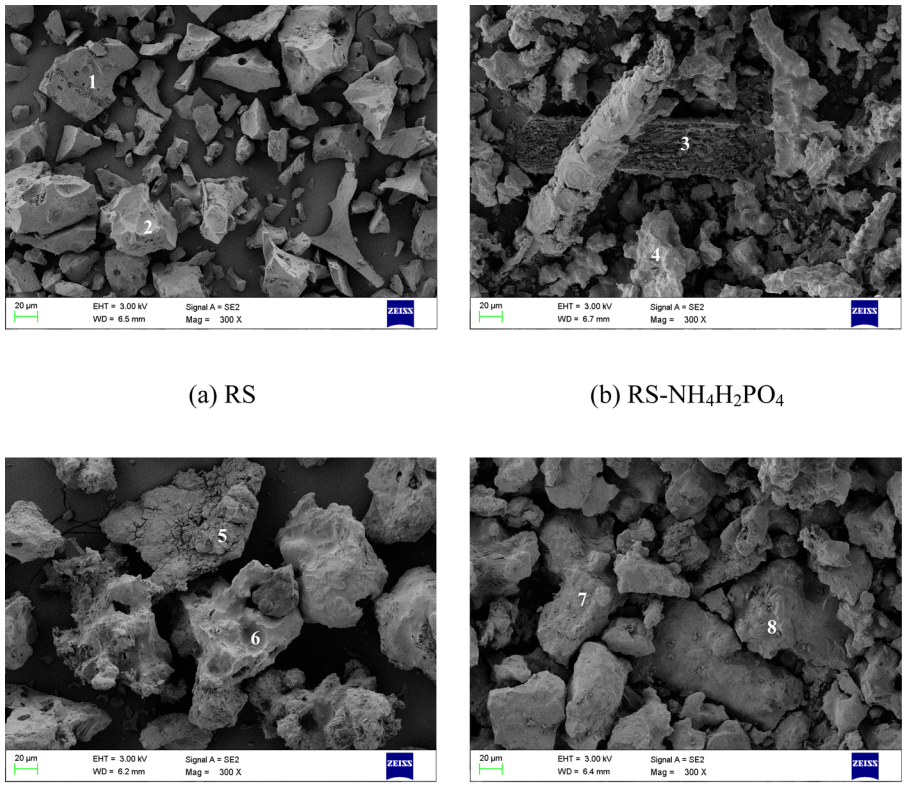

(a) RS (b) RS-$NH_4H_2PO_4$

(c) CS (d) CS-$NH_4H_2PO_4$

Figure 7. SEM micrographs of the formed samples after heating at 1000 °C.

Table 3. EDS Spot Analysis Results Referring to Figure 7 (wt %)

	RS		RS−$NH_4H_2PO_4$		CS		CS−$NH_4H_2PO_4$	
element	1	2	3	4	5	6	7	8
K	10.11	11.75	11.31	10.39	15.11	9.52	14.16	10.72
Na	1.00	0.96	0.00	0.77	2.19	1.33	0.75	4.45
Mg	1.31	1.65	1.21	0.78	1.15	3.03	0.62	2.05
Ca	2.26	5.93	1.88	1.44	9.06	5.85	2.85	5.04
Al	0.00	0.00	0.00	0.00	1.26	5.31	2.14	3.98
Fe	0.00	0.00	0.00	0.00	4.60	7.92	2.55	2.34
Si	39.96	31.58	35.74	29.05	32.58	23.23	14.43	10.23
P	0.0	2.00	7.96	7.32	0.00	0.00	23.54	18.04
O	45.36	46.13	41.92	50.25	34.06	43.80	37.99	42.57
C	0.00	0.00	0.00	0.00	0.00	0.00	0.95	0.59

ashes of RS and CS and the raw materials mixed with $NH_4H_2PO_4$ with the molar ratio of 1:1 PO_4^{3-}/K at 1000 °C. The micrographs of the individual ash samples illustrated in panels a and c of Figure 7 show different degrees of fusion and resolidification. The ash of RS is completely melted together and adhered to the bottom of the alumina boat at 1000 °C. The RS ash needs to be crushed into pieces and ground prior to the SEM analyses. The surface of the sample is smooth with sharp edges because of the crush effect. The ash of CS is isolated partly melted, which contains agglomerated particles. Some of the surface seems to be rough, and some of it is smooth. Voids with round rims of different sizes are visible in the melted RS and CS ashes. The voids represent the formation of bubbles because of decomposition of salts (mainly carbonates) and release of gases as the ash melted severely in a liquid phase with high surface tensions.[30] As demonstrated in panels b and d of Figure 7, a significant effect of $NH_4H_2PO_4$ on the microcosmic structure is noticed and the ashes of the mixture show quite different morphologies. The ash of RS with $NH_4H_2PO_4$ is melted and agglomerated but that does not yet undergo any great fusion. Only a slight melting layer is observed to cover the surface of the sample. However, the surface of the ash of CS with $NH_4H_2PO_4$ is rough with loose structures and does not exhibit any significant fusion and agglomeration.

Every two of the representative areas from panels a−d of Figure 7 are chosen for EDS spot analysis shown in Table 3. As revealed by EDS analyses, K and Si are two dominant elements detected in the fused spots 1 and 2 from the ash of RS. Such element composition and correlation indicate the formation of potassium silicates. Some of the potassium silicates and eutectics of them have melting points as low as 600 °C, which will lead to the melted ash at elevated temperatures.[29]

DOI: 10.1021/acs.energyfuels.5b00285
Energy Fuels 2015, 29, 2555−2563

The absence of crystalline phases of potassium compounds identified by XRD in the RS ash at 1000 °C can be explained by the formation of potassium silicates with low melting points, which are amorphous and cannot be detected by XRD. Besides K and Si, high contents of Ca, Al, and Fe are detected in spot 5 and 6 of CS ash. This is consistent with the existence of K−Al silicates and K−Fe silicates identified by XRD, which make the melting point higher than the RS ash. The addition of $NH_4H_2PO_4$ introduces more P in the ashes of RS and CS, which can be seen from the significant increased content of P in spot 3, 4, 7, and 8. Therefore, the morphology transformation of the ashes is mainly due to the formation of phosphorus compounds compared to the elemental contents of the individual ash samples. Together with the XRD results, the EDS analyses confirm that PO_4^{3-} from ammonium phosphates can react with potassium and dissolve in the melt. The formation of the high-melting-point potassium phosphates will improve the sintering behaviors of the ashes.

4. CONCLUSION

The influence of ammonium phosphates, i.e., $NH_4H_2PO_4$ and $(NH_4)_2HPO_4$, on gaseous potassium release was studied in a tube furnace. The addition of $NH_4H_2PO_4$ and $(NH_4)_2HPO_4$ both decrease the gaseous potassium release ratio and show the same trends. $NH_4H_2PO_4$ and $(NH_4)_2HPO_4$ can be more effective with a higher initial potassium content. The release ratios of RS with $NH_4H_2PO_4$ and $(NH_4)_2HPO_4$ are 12.1 and 13.2% at 1000 °C, respectively, which both decrease most compared to the ratio of RS. The release ratio decreases as the PO_4^{3-}/K ratio increases from 0.5:1 to 4:1 at every temperature. Ammonium phosphates need to be excessive to capture potassium in the ash significantly. The appropriate molar ratios of PO_4^{3-}/K are between 1:1 and 2:1, considering the negative influences caused by too much excessive ammonium phosphates.

The ash-forming characteristics were investigated by visual evaluation, XRD, and SEM−EDS analyses. Surface melting and sintering are inhibited by the addition of $NH_4H_2PO_4$ and $(NH_4)_2HPO_4$ according to the appearance of the formed ashes. Ammonium phosphates can react with potassium to form potassium phosphates and potassium calcium phosphates that bound potassium in a K−Ca−P ternary system, which will not be influenced by the other ash-forming elements, i.e., Mg and Fe, at elevated temperatures. A significant effect of $NH_4H_2PO_4$ on the microcosmic structure is noticed, and the ashes of the mixture show quite different morphologies because of the formation of phosphorus compounds. These phosphates, including $K_2CaP_2O_7$, K_3PO_4, and $KCaPO_4$, are high-melting-point compounds contributed to retaining potassium and preventing sintering of the formed ash.

AUTHOR INFORMATION

Corresponding Author

*Telephone: +86-531-88392414. Fax: +86-531-88392701. E-mail: hankh@163.com.

Notes

The authors declare no competing financial interest.

ACKNOWLEDGMENTS

This study was supported by the National Natural Science Foundation of China (51206096) and the College Independent Innovation Fund of Jinan (201401275).

REFERENCES

(1) McKendry, P. Energy production from biomass (Part 2): Conversion technologies. *Bioresour. Technol.* **2002**, *83* (1), 47−54.
(2) Balat, M.; Balat, M.; Kırtay, E.; Balat, H. Main routes for the thermo-conversion of biomass into fuels and chemicals. Part 1: Pyrolysis systems. *Energy Convers. Manage.* **2009**, *50* (12), 3147−3157.
(3) Jayaraman, K.; Goekalp, I. Pyrolysis, combustion and gasification characteristics of miscanthus and sewage sludge. *Energy Convers. Manage.* **2015**, *89*, 83−91.
(4) Tekin, K.; Karagoz, S.; Bektas, S. A review of hydrothermal biomass processing. *Renewable Sustainable Energy Rev.* **2014**, *40*, 673−687.
(5) Du, S. W.; Chen, W. H.; Lucas, J. A. Pretreatment of biomass by torrefaction and carbonization for coal blend used in pulverized coal injection. *Bioresour. Technol.* **2014**, *161*, 333−339.
(6) Werther, J.; Saenger, M.; Hartge, E.-U.; Ogada, T.; Siagi, Z. Combustion of agricultural residues. *Prog. Energy Combust.* **2000**, *26* (1), 1−27.
(7) Saidur, R.; Abdelaziz, E. A.; Demirbas, A.; Hossain, M. S.; Mekhilef, S. A review on biomass as a fuel for boilers. *Renewable Sustainable Energy Rev.* **2011**, *15* (5), 2262−2289.
(8) Demirbas, A. Potential applications of renewable energy sources, biomass combustion problems in boiler power systems and combustion related environmental issues. *Prog. Energy Combust.* **2005**, *31* (2), 171−192.
(9) Hupa, M. Ash-related issues in fluidized-bed combustion of biomasses: Recent research highlights. *Energy Fuels* **2012**, *26* (1), 4−14.
(10) Antunes, R. A.; Lopes de Oliveira, M. C. Corrosion in biomass combustion: A materials selection analysis and its interaction with corrosion mechanisms and mitigation strategies. *Corros. Sci.* **2013**, *76*, 6−26.
(11) Vassilev, S. V.; Baxter, D.; Vassileva, C. G. An overview of the behavior of biomass during combustion: Part II. Ash fusion and ash formation mechanisms of biomass types. *Fuel* **2014**, *117*, 152−183.
(12) Boström, D.; Skoglund, N.; Grimm, A.; Boman, C.; Öhman, M.; Broström, M.; Backman, R. Ash transformation chemistry during combustion of biomass. *Energy Fuels* **2012**, *26* (1), 85−93.
(13) Piotrowska, P.; Zevenhoven, M.; Hupa, M.; Giuntoli, J.; de Jong, W. Residues from the production of biofuels for transportation: Characterization and ash sintering tendency. *Fuel Process. Technol.* **2013**, *105*, 37−45.
(14) Liao, Y.; Yang, G.; Ma, X. Experimental study on the combustion characteristics and alkali transformation behavior of straw. *Energy Fuels* **2012**, *26* (2), 910−916.
(15) Niu, Y.; Du, W.; Tan, H.; Xu, W.; Liu, Y.; Xiong, Y.; Hui, S. Further study on biomass ash characteristics at elevated ashing temperatures: The evolution of K, Cl, S and the ash fusion characteristics. *Bioresour. Technol.* **2013**, *129*, 642−645.
(16) Glazer, M. P.; Khan, N. A.; de Jong, W.; Spliethoff, H.; Schurmann, H.; Monkhouse, P. Alkali metals in circulating fluidized bed combustion of biomass and coal: Measurements and chemical equilibrium analysis. *Energy Fuels* **2005**, *19* (5), 1889−1897.
(17) Khan, A. A.; de Jong, W.; Jansens, P. J.; Spliethoff, H. Biomass combustion in fluidized bed boilers: Potential problems and remedies. *Fuel Process. Technol.* **2009**, *90* (1), 21−50.
(18) Niu, Y.; Zhu, Y.; Tan, H.; Hui, S.; Jing, Z.; Xu, W. Investigations on biomass slagging in utility boiler: Criterion numbers and slagging growth mechanisms. *Fuel Process. Technol.* **2014**, *128*, 499−508.
(19) Chaivatamaset, P.; Sricharoon, P.; Tia, S.; Bilitewski, B. A prediction of defluidization time in biomass fired fluidized bed combustion. *Appl. Therm. Eng.* **2013**, *50* (1), 722−731.
(20) Johansen, J. M.; Jakobsen, J. G.; Frandsen, F. J.; Glarborg, P. Release of K, Cl, and S during pyrolysis and combustion of high-chlorine biomass. *Energy Fuels* **2011**, *25* (11), 4961−4971.
(21) Enestam, S.; Bankiewicz, D.; Tuiremo, J.; Mäkelä, K.; Hupa, M. Are NaCl and KCl equally corrosive on superheater materials of steam boilers? *Fuel* **2013**, *104*, 294−306.

DOI: 10.1021/acs.energyfuels.5b00285
Energy Fuels 2015, 29, 2555−2563

(22) Díaz-Ramírez, M.; Frandsen, F. J.; Glarborg, P.; Sebastián, F.; Royo, J. Partitioning of K, Cl, S and P during combustion of poplar and brassica energy crops. *Fuel* **2014**, *134*, 209−219.
(23) Kassman, H.; Pettersson, J.; Steenari, B. M.; Åmand, L. E. Two strategies to reduce gaseous KCl and chlorine in deposits during biomass combustion—Injection of ammonium sulphate and co-combustion with peat. *Fuel Process. Technol.* **2013**, *105*, 170−180.
(24) Aho, M.; Ferrer, E. Importance of coal ash composition in protecting the boiler against chlorine deposition during combustion of chlorine-rich biomass. *Fuel* **2005**, *84* (2−3), 201−212.
(25) Elled, A. L.; Davidsson, K. O.; Åmand, L. E. Sewage sludge as a deposit inhibitor when co-fired with high potassium fuels. *Biomass Bioenergy* **2010**, *36* (11), 1546−1554.
(26) Skoglund, N.; Grimm, A.; Öhman, M.; Boström, D. Effects on ash chemistry when co-firing municipal sewage sludge and wheat straw in a fluidized bed: Influence on the ash chemistry by fuel mixing. *Energy Fuels* **2013**, *27* (10), 5725−5732.
(27) Tran, K. Q.; Iisa, K.; Steenari, B. M.; Lindqvist, O. A kinetic study of gaseous alkali capture by kaolin in the fixed bed reactor equipped with an alkali detector. *Fuel* **2005**, *84* (2−3), 169−175.
(28) Konsomboon, S.; Pipatmanomai, S.; Madhiyanon, T.; Tia, S. Effect of kaolin addition on ash characteristics of palm empty fruit bunch (EFB) upon combustion. *Appl. Energy* **2011**, *88* (1), 298−305.
(29) Wang, L.; Skreiberg, O.; Becidan, M. Investigation of additives for preventing ash fouling and sintering during barley straw combustion. *Appl. Therm. Eng.* **2014**, *70* (2), 1262−1269.
(30) Wang, L.; Becidan, M.; Skreiberg, O. Sintering behavior of agricultural residues ashes and effects of additives. *Energy Fuels* **2012**, *26* (9), 5917−5929.
(31) Steenari, B. M.; Lindqvist, O. High-temperature reactions of straw ash and the anti-sintering additives kaolin and dolomite. *Biomass Bioenergy* **1998**, *14* (1), 67−76.
(32) Steenari, B. M.; Lundberg, A.; Pettersson, H.; Wilewska-Bien, M.; Andersson, D. Investigation of ash sintering during combustion of agricultural residues and the effect of additives. *Energy Fuels* **2009**, *23*, 5655−5662.
(33) Boström, D.; Eriksson, G.; Boman, C.; Öhman, M. Ash transformations in fluidized-bed combustion of rapeseed meal. *Energy Fuels* **2009**, *23*, 2700−2706.
(34) Grimm, A.; Skoglund, N.; Boström, D.; Öhman, M. Bed agglomeration characteristics in fluidized quartz bed combustion of phosphorus-rich biomass fuels. *Energy Fuels* **2011**, *25* (3), 937−947.
(35) Grimm, A.; Skoglund, N.; Boström, D.; Boman, C.; Öhman, M. Influence of phosphorus on alkali distribution during combustion of logging residues and wheat straw in a bench-scale fluidized bed. *Energy Fuels* **2012**, *26* (5), 3012−3023.
(36) Li, L.; Ren, Q.; Li, S.; Lu, Q. Effect of phosphorus on the behavior of potassium during the co-combustion of wheat straw with municipal sewage sludge. *Energy Fuels* **2013**, *27* (10), 5923−5930.
(37) Skoglund, N.; Grimm, A.; Öhman, M.; Boström, D. Combustion of biosolids in a bubbling fluidized bed, part 1: Main ash-forming elements and ash distribution with a focus on phosphorus. *Energy Fuels* **2014**, *28* (2), 1183−1190.
(38) Fryda, L.; Panopoulos, K.; Vourliotis, P.; Pavlidou, E.; Kakaras, E. Experimental investigation of fluidised bed co-combustion of meat and bone meal with coals and olive bagasse. *Fuel* **2006**, *85* (12−13), 1685−1699.
(39) Wu, H.; Castro, M.; Jensen, P. A.; Frandsen, F. J.; Glarborg, P.; Dam-Johansen, K.; Røkke, M.; Lundtorp, K. Release and transformation of inorganic elements in combustion of a high-phosphorus fuel. *Energy Fuels* **2011**, *25* (7), 2874−2886.
(40) Knudsen, J. N.; Jensen, P. A.; Dam-Johansen, K. Transformation and release to the gas phase of Cl, K, and S during combustion of annual biomass. *Energy Fuels* **2004**, *18* (5), 1385−1399.
(41) Krishnarao, R. V.; Subrahmanyam, J.; Kumar, T. J. Studies on the formation of black particles in rice husk silica ash. *J. Eur. Ceram. Soc.* **2001**, *21* (1), 99−104.
(42) Novakovic, A.; van Lith, S. C.; Frandsen, F. J.; Jensen, P. A.; Holgersen, L. B. Release of potassium from the systems K−Ca−Si and K−Ca−P. *Energy Fuels* **2009**, *23* (7), 3423−3428.
(43) Javed, M. T.; Irfan, N.; Gibbs, B. M. Control of combustion-generated nitrogen oxides by selective non-catalytic reduction. *J. Environ. Manage.* **2007**, *83* (3), 251−289.

DOI: 10.1021/acs.energyfuels.5b00285
Energy Fuels 2015, 29, 2555−2563